Non-Zeeman splitting for a spin-resolved STM with a Kondo adatom in a spin-polarized two-dimensional electron gas

A. C. Seridonio,[1] F. S. Orahcio,[2] F. M. Souza,[3] and M. S. Figueira[2]

[1]*Departamento de Física e Química, Universidade Estadual Paulista "Júlio de Mesquita Filho," 15385-000, Ilha Solteira, SP, Brazil*

[2]*Instituto de Física, Universidade Federal Fluminense, 24210-340 Niterói, RJ, Brazil*

[3]*Instituto de Física, Universidade Federal de Uberlândia, 38400-902, Uberlândia, MG, Brazil*

(Received 14 July 2011; revised manuscript received 8 February 2012; published 6 April 2012)

We theoretically investigate the spin-resolved local density of states (SR-LDOS) of a spin-polarized two-dimensional electron gas in the presence of a Kondo adatom and a scanning tunneling microscopy probe. Using Green's function formalism and the atomic approach in the limit of infinite Coulomb correlation, an analytical SR-LDOS expression in the low-temperature regime of the system is found. This formal result is given in terms of phase shifts originated by the adatom scattering and Fano interference. The SR-LDOS is investigated as a function of the probe position and different Fano factors. Our findings provide an alternative way to spin split the Kondo resonance without the use of huge magnetic fields, typically necessary in adatom systems characterized by large Kondo temperatures. We observe a non-Zeeman spin splitting of the Kondo resonance in the total LDOS, with one spin component pinned around the host Fermi level. Interestingly, this result is in accordance to recent experimental data [Phys. Rev. B **82**, 020406R (2010)].

DOI: 10.1103/PhysRevB.85.165109 PACS number(s): 72.25.−b, 73.23.−b, 74.55.+v, 75.20.Hr

I. INTRODUCTION

The scattering of electrons by a magnetic impurity in a metallic environment is responsible for the manifestation of the Kondo effect.[1] This phenomenon occurs as a result of an antiferromagnetic coupling between the localized spin at the impurity and the surrounding conduction electrons of the host. In particular, at temperatures much lower than the Kondo temperature T_K, an electron cloud emerges to screen the magnetic moment placed at the impurity site. Thus, a sharp resonance pinned at the Fermi energy appears in the impurity density of states and characterizes the formation of the Kondo peak. Such an effect was first observed in resistivity measurements of magnetic alloys, later in transport properties of quantum dots (QDs) performed in a two-dimensional electron gas (2DEG).[2–11] More recently, Kondo effect was also measured using scanning tunneling microscopy (STM) in the presence of impurities deposited on metallic surfaces.[12–27]

In the context of unpolarized scanning tunneling microscopy probes, the conductance exhibits the Fano line shape due to the quantum interference between the transport channels given by the conduction bands and the adatom.[24–29] Additionally, for STM probes not very close to the metallic host and in the low-temperature regime, the STM device probes the local density of states (LDOS) of the sample.

In the case of spin-polarized STM probes, interesting new features emerge as the spin splitting of the Fano-Kondo profile of the conductance and the Fano-Kondo spin filter.[30–33] In this scenario, several experimental and theoretical works discuss related phenomena employing ferromagnetic leads coupled to QDs and adatoms.[34–55] In particular, in the emerging field of spintronics, the interplay between the Fano-Kondo effect and the ferromagnetism of a metallic environment plays a crucial role in the manufacturing of novel spintronics devices.

In this work, we report an analytical description of the spin-resolved local density of states (SR-LDOS) for an unpolarized STM probe, hybridized with a single Kondo adatom in a ferromagnetic (FM) island, considered here as a spin-polarized two-dimensional electron gas (SP-2DEG). Such analysis is done in the framework of the single impurity Anderson model[56] (SIAM), using the atomic approach with infinite Coulomb correlation[57–59] in order to determine the adatom Green's function (GF).

The main result of our simulations is the emergence of an asymmetric spin splitting in the Kondo peak, which agrees with some experimental works.[34,45,47,49,50] Here, we highlight the experiment done by Kawahara *et al.*,[49] where the measured LDOS shows that one spin channel has a Kondo peak pinned at the vicinity of the host Fermi level, while the opposite is shifted by the spin polarization of the 2DEG forming the island surface. We note that the behavior we see here is not similar to the usual Zeeman splitting due to an external magnetic field.[2,3,6,7,23] In the present model, there are no external fields.

Contrary to the QD systems, where the Kondo temperature is of the order of milliKelvin and the temperature could be tuned to observe the suppression of the Kondo resonance, in most STM systems,[60] the Kondo temperature is of the order of tens of Kelvin and the experimental STM setups do not allow the temperature variation in such a range to observe the evolution of the Kondo effect. On the other hand, to verify the splitting of the Kondo peak in STM experiments, it is necessary to apply a magnetic field of hundreds of Tesla, which is not feasible. Thus, the type of experiment proposed in our work could be useful to produce a splitting of the Kondo resonance without huge magnetic fields.

This paper is organized as follows. In Sec. II, we show the theoretical model for the STM in terms of the Anderson Hamiltonian. We derive in Sec. III the SR-LDOS formula with and without a STM probe. For both cases in the low-temperature limit, we show that the SR-LDOS expression can be labeled by phase shifts due to the adatom scattering and Fano interference. In Sec. IV, we discuss the results of the host Fano parameter, which displays spin-polarized Friedel oscillations[61–63] and we present a wide analysis of

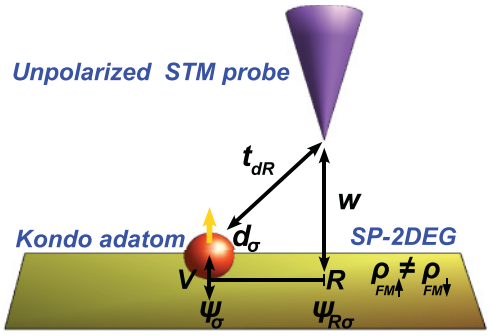

FIG. 1. (Color online) STM device composed by an unpolarized probe and a Kondo adatom hybridized to a SP-2DEG. The parameters V, t_{dR}, and w are hopping terms. The letters d_σ, Ψ_σ, and $\Psi_{R\sigma}$ denote, respectively, the fermionic annihilation operators to the adatom, to the site of the host side coupled to the adatom, and to the site just below the probe.

the SR-LDOS as a function of the bias voltage for different probe positions and Fano factors. The atomic approach is employed considering an infinite Coulomb correlation in order to calculate the adatom GF. We apply our formulation in Sec. V to describe the Kondo peak splitting found in the experiment of Ref. 49. The conclusions appear in Sec. VI, and in the Appendices, we give details of the derivations of the atomic GF for the adatom as well as for the host Fano factor.

II. THEORETICAL MODEL

A. Hamiltonian

In Fig. 1, we represent an unpolarized STM probe coupled to the FM island hybridized to the Kondo adatom deposited on its surface. Note that when the hopping term $t_{dR} \gg w$, the setup behaves as a single-electron transistor (SET),[2,3] which we call *peak limit*, due to the emergence of the Kondo resonance in the LDOS energy profile as we shall see. The other limit we call *dip limit*; it comprises the cases $t_{dR} \ll w$ and $t_{dR} \simeq w$, which resemble the T-shaped QD device[7] characterized by a Fano-Kondo dip.

The system we investigated is described according to the Hamiltonian

$$\mathcal{H} = \mathcal{H}_{\rm FM} + \mathcal{H}_{\rm probe} + \sum_\sigma h^\sigma_{\rm tun}. \tag{1}$$

The first term represents the SIAM (Ref. 56)

$$\mathcal{H}_{\rm FM} = \sum_{\vec{k}\sigma} \varepsilon_{k\sigma} c^\dagger_{\vec{k}\sigma} c_{\vec{k}\sigma} + \sum_\sigma E_d d^\dagger_\sigma d_\sigma + \sum_{\vec{k}\sigma} V_{dk\sigma}(c^\dagger_{\vec{k}\sigma} d_\sigma + d^\dagger_\sigma c_{\vec{k}\sigma}) + U d^\dagger_\uparrow d_\uparrow d^\dagger_\downarrow d_\downarrow \tag{2}$$

that assumes the island as a SP-2DEG described by the operator $c^\dagger_{\vec{k}\sigma}$ ($c_{\vec{k}\sigma}$) for the creation (annihilation) of an electron in a quantum state labeled by the wave vector $\vec{k}$, spin σ, and energy

$$\varepsilon_{k\sigma} = D_\sigma k^{-1}_{F\sigma}(k - k_{F\sigma}) \tag{3}$$

which depends on the spin-polarized band half-widths D_σ forming the host Fermi sea and the wave numbers $k_{F\sigma}$ evaluated at the Fermi energy $\varepsilon_F \equiv 0$.

For the adatom, $d^\dagger_\sigma$ (d_σ) creates (annihilates) one electron with spin σ in state E_d. The third term hybridizes the adatom level and the host continuum of states. The coupling matrix element is modeled as

$$V_{dk\sigma} = \frac{V}{\sqrt{N_{\rm FM\sigma}}} \frac{\Gamma^2}{\Gamma^2 + \varepsilon^2_{k\sigma}}, \tag{4}$$

which obeys a Lorentzian behavior for a sake of simplicity to mimic a nonlocal coupling between the adatom and the island. $N_{\rm FM\sigma}$ is the number of conduction states for a given spin and Γ is the width of this interaction around ε_F. Coulomb correlation between two electrons with opposite spins at the adatom site is also taken into account and is represented by the letter U. For simplicity, we consider the U infinite version of the atomic approach[57,58] that gives the adatom GF. In particular, taking the limit $\Gamma \gg \varepsilon_{k\sigma}$ in Eq. (4), we obtain a constant $V_{dk\sigma}$, i.e., $V_{dk\sigma} = \frac{V}{\sqrt{N_{\rm FM\sigma}}}$. This corresponds to the case of a site of the FM island side coupled to the adatom, which we designate local coupling. We mention that Eqs. (3) and (4) were previously applied in the context of unpolarized bulk electrons in a system described by the Kondo model.[62] In this work, we employ the Lorentzian shape to emulate the nonlocality of the adatom-island coupling.

The FM island is considered a spin-polarized electron bath, with polarization given by

$$P = \frac{\rho_{\rm FM\uparrow} - \rho_{\rm FM\downarrow}}{\rho_{\rm FM\uparrow} + \rho_{\rm FM\downarrow}}, \tag{5}$$

where

$$\rho_{\rm FM\sigma} = \frac{1}{2D_\sigma} \tag{6}$$

is the host density of states in the flat band approximation. This quantity is expressed in terms of

$$D_\sigma = \frac{D_0}{(1 + \sigma P)} \tag{7}$$

for a given spin σ and the unpolarized density

$$\rho_0 = \frac{1}{2D_0}, \tag{8}$$

written in terms of the width D_0. The unpolarized part of the system is the conduction band given by the Hamiltonian

$$\mathcal{H}_{\rm probe} = \sum_{\vec{p}\sigma} \varepsilon_p b^\dagger_{\vec{p}\sigma} b_{\vec{p}\sigma}, \tag{9}$$

which corresponds to the second term in Eq. (1) for free electrons in the STM probe. Such conduction electrons are ruled by fermionic operators $b^\dagger_{\vec{p}\sigma}$ and $b_{\vec{p}\sigma}$. To perform the coupling between Eqs. (2) and (9), we have to define

$$h^\sigma_{\rm tun} = \sum_{\vec{p}} b^\dagger_{\vec{p}\sigma}(w\Psi_{R\sigma} + t_{dR} d_\sigma + {\rm H.c.}) \tag{10}$$

as the spin tunneling Hamiltonian that hybridizes the STM probe conduction states with those in the island and the adatom.

The former hopping parameter we consider proportional to the energy-independent term w, with the fermionic operator

$$\Psi_{R\sigma} = \frac{1}{\sqrt{N_{\mathrm{FM}\sigma}}} \sum_{\vec{k}} e^{i\vec{k}.\vec{R}} c_{\vec{k}\sigma}, \tag{11}$$

which describes a conduction state at the site $\vec{R}$ laterally displaced from the adatom. This operator admits an expansion in plane waves due to the assumption of an infinite 2DEG forming the island surface. The second hybridization parameter in Eq. (10) is proportional to the adatom operator d_σ and the spatial-dependent hopping

$$t_{dR} = t_{do} \exp(-k_F R), \tag{12}$$

which provides a decreasing STM probe-adatom coupling. This characteristic ensures a vanishing behavior for huge lateral displacements, which was already employed in the literature,[14,31,32]

B. Atomic approach

In order to implement the atomic approach,[57–59] we consider the adatom-island coupling as local. Thus, we begin

$$\mathcal{H}_{\mathrm{FM}} = \sum_{\vec{k}\sigma} \varepsilon_{k\sigma} c^{\dagger}_{\vec{k}\sigma} c_{\vec{k}\sigma} + \sum_{\sigma} E_d X_{d,\sigma\sigma} + V(X^{\dagger}_{d,0\sigma} \Psi_\sigma + \Psi^{\dagger}_\sigma X_{d,0\sigma}), \tag{13}$$

which is derived from Eq. (2) taking into account $V_{dk\sigma} = \frac{V}{\sqrt{N_{\mathrm{FM}\sigma}}}$. Here, $X_{a,b}$ is the Hubbard operator[64,65] that projects out the doubly occupied state from the adatom to ensure the limit of infinite Coulomb correlation, where the label (a,b) defines the parameters associated with the corresponding atomic transition and Ψ_σ is $\Psi_{R\sigma}$ [Eq. (11)] evaluated at the origin. This Hamiltonian is useful for the calculation of the adatom GF and, consequently, the system SR-LDOS.

This GF is based on an extension of the Hubbard cumulant expansion also applicable to the Anderson lattice with impurity-host couplings treated as perturbations.[65] The use of this expansion allows us to express the exact GF in terms of an unknown effective cumulant. In a previous work, the Anderson lattice was studied with an approximate effective cumulant obtained from the atomic limit of the model in a procedure called the zero band width (ZBW) approximation. The advantage is that such method includes all the higher-order cumulants absent in the previous diagrammatic calculations.[65]

The method presents some similarities to the exact diagonalization (ED) for the SIAM. The ED is a brute-force method to solve the Hamiltonian treated as a discrete bath by considering the impurity coupled to a finite number of conduction sites (N_c) of the host band. In principle, it is an exact method as the name implies, but its limitation relies in the number of conduction sites considered, and the Hilbert space grows extremely fast when N_c is enlarged. The cumulant approach is not equivalent to the ED; it allows us to derive the adatom GF from the Anderson lattice model in the atomic limit.[66] This GF is related to the conduction band GF, which depends on the atomic level that represents the band. Such a level is the starting point for the ZBW approximation. The ZBW is a mapping of the system Hamiltonian onto an effective tight-binding chain with only two sites, one for the adatom discrete energy and other for the band atomic level. Then, employing the Lehmann representation, the atomic GF for the impurity is calculated as well as the approximated cumulants. They determine the full GF in such a way that the Friedel sum rule should be satisfied by the band atomic level. In particular, this GF does not present a spurious oscillatory behavior in the Kondo peak as that observed by the standard ED method. In the ED context, this artifact can be solved by the *self-energy trick*.[55] We also would like to mention that the atomic approach could be easily generalized to the multiorbital Anderson model because once the atomic solution is known, the method follows the same steps realized in the spin $S = 1/2$ SIAM.

To obtain the exact GF of an Anderson impurity (adatom), we can employ the chain approximation,[65] but considering all the possible cumulants in the expansion for the Anderson lattice. Similarly to the Feynman diagrams, it is possible to rearrange all those that contribute to the exact adatom GF by defining an effective cumulant, determined by all the diagrams that can not be separated by cutting a single edge ("proper" or "irreducible" diagrams).

As we are interested in the exact GF for the adatom, we use the standard definition

$$\mathcal{G}^{dd}_\sigma(\tau) = -\frac{i}{\hbar}\theta(\tau)\mathrm{Tr}\{\varrho_{\mathrm{FM}}[d_\sigma(\tau), d^{\dagger}_\sigma(0)]_+\} \tag{14}$$

in time coordinate, where $\hbar$ is the Planck constant h divided by 2π, $\theta(\tau)$ the step function at the instant τ, Tr the trace over the eigenstates of the Hamiltonian in Eq. (2), ϱ_{FM} the density matrix of the FM island, and $[\ldots,\ldots]_+$ is the anticommutator between the adatom operators at different times.

The time Fourier transformation of Eq. (14) thus provides the adatom GF in energy coordinate, which is then obtained by replacing the bare cumulant for the effective one calculated by following the atomic approach with the Hamiltonian in Eq. (13). As a result, we have

$$\mathcal{G}^{dd}_\sigma(\omega) = \frac{\mathcal{M}^{\mathrm{eff}}_\sigma(\omega)}{1 - \mathcal{M}^{\mathrm{eff}}_\sigma(\omega)|V|^2 \sum_{\vec{k}} \mathcal{G}^{c}_\sigma(\vec{k},\omega)} \tag{15}$$

as the adatom GF in terms of the effective cumulant $\mathcal{M}^{\mathrm{eff}}_\sigma(\omega)$ and the free-electron GF

$$\mathcal{G}^{c}_\sigma(\vec{k},\omega) = \frac{1}{\omega - \varepsilon_{\vec{k}\sigma} + i\eta}, \tag{16}$$

where $\eta \to 0^+$. The atomic version of Eq. (15) is given by (see Appendix A)

$$\mathcal{G}^{dd}_{\mathrm{at},\sigma}(\omega) = \frac{\mathcal{M}^{\mathrm{at}}_\sigma(\omega)}{1 - \mathcal{M}^{\mathrm{at}}_\sigma(\omega)|V|^2 \mathcal{G}^{\mathrm{ZBW}}_\sigma(\omega)}, \tag{17}$$

which results in

$$\mathcal{M}^{\mathrm{at}}_\sigma(\omega) = \frac{\mathcal{G}^{dd}_{\mathrm{at},\sigma}(\omega)}{1 + \mathcal{G}^{dd}_{\mathrm{at},\sigma}(\omega)|V|^2 \mathcal{G}^{\mathrm{ZBW}}_\sigma(\omega)} \tag{18}$$

for the effective cumulant determined from the adatom GF calculated in Appendix A, both dependent on

$$\mathcal{G}^{\mathrm{ZBW}}_\sigma(\omega) = \frac{1}{\omega - (\varepsilon_{0\sigma} - \mu) + i\eta} \tag{19}$$

for an electron state in the ZBW approximation with μ to denote the FM island chemical potential. As we can see, Eq. (19) replaces all energy contributions of the original Fermi

sea by two spin-dependent atomic levels, i.e., we perform the substitution $\sum_{\vec{k}\sigma} \varepsilon_{k\sigma} c^{\dagger}_{\vec{k}\sigma} c_{\vec{k}\sigma} \rightarrow \sum_{\sigma} \varepsilon_{0\sigma} c^{\dagger}_{0\sigma} c_{0\sigma}$ in Eq. (13) with $\varepsilon_{k\sigma} = \varepsilon_{0\sigma}$ representing the band atomic level for a given spin σ. As this procedure overestimates the coupling of the spin-polarized conduction bands of the island with the adatom due to the concentration of the bands at atomic levels, we have to moderate this effect,[66] performing the substitution of V^2 by Δ^2 in Eqs. (17) and (18), where $\Delta = \pi V^2 \rho_0$ is the Anderson parameter.

To determine the adatom GF, we use the atomic cumulant $\mathcal{M}^{\rm at}_{\sigma}(\omega)$ as effective in Eq. (15) and verify that

$$\mathcal{G}^{dd}_{\sigma}(\omega) = \frac{\mathcal{M}^{\rm at}_{\sigma}(\omega)}{1 - \mathcal{M}^{\rm at}_{\sigma}(\omega)\frac{|V|^2}{2D_{\sigma}} \ln\left(\frac{\omega + D_{\sigma} + \mu}{\omega - D_{\sigma} + \mu}\right)} \tag{20}$$

provides an analytical expression in the flat band approximation. We mention that $\mathcal{M}^{\rm at}_{\sigma}(\omega)$ is a simplification, but it contains all the diagrams that should be presented in such a way that the correspondent GF displays realistic features.

As the final step of the atomic approach implementation, we have to find adequate values of the atomic levels $\varepsilon_{0\sigma}$ that well describe the ZBW GFs in Eq. (19) and consequently the adatom GF. To that end, we use the condition that, in metallic systems, the most important region for conduction electrons is placed at the Fermi energy ε_F, and that the coupling to an Anderson impurity leads to the Friedel's sum rule[67]

$$\rho_{d,\sigma}(\varepsilon_F) = -\frac{1}{\pi}{\rm Im}\left\{\mathcal{G}^{dd}_{\sigma}(\varepsilon_F)\right\} = \frac{\sin^2[\delta_{\sigma}(\varepsilon_F)]}{\pi \Delta_{\sigma}} \tag{21}$$

for the adatom spectral density. Here, $\delta_{\sigma}(\varepsilon_F) = \pi n_{d,\sigma}$ is the conduction phase shift at the Fermi level, Im represents the imaginary part, $\Delta_{\sigma} = \Delta(1 + \sigma P)$ is the spin-dependent Anderson parameter, and $n_{d,\sigma}$ is the adatom occupation with spin σ. Thus, we find the atomic levels $\varepsilon_{0\sigma}$ calculating self-consistently Eq. (21) together with

$$n_{d,\sigma} = \langle X_{d,\sigma\sigma} \rangle = -\frac{1}{\pi}\int_{-\infty}^{+\infty} d\omega\, {\rm Im}\left\{\mathcal{G}^{dd}_{\sigma}(\omega)\right\} n_F(\omega). \tag{22}$$

In Eq. (22), $n_F(\omega)$ is the Fermi-Dirac distribution.

It is important to emphasize here that the choice of the atomic approach to calculate the adatom GF is only due to its computational simplicity and ability to obtain the Kondo peak, but we must take into account that the method presents some limitations that were extensively discussed in the original papers.[57–59] The SR-LDOS formulas obtained in Sec. III are general; we could employ other more powerful and precise techniques to calculate the GF of the Anderson impurity, such as the numerical renormalization group[10,11,68] (NRG) without any modifications in the formalism.

III. SR-LDOS

A. SR-LDOS in the scheme of phase shifts for the FM island

In this section we derive at the temperature range $T \ll T_K$ the SR-LDOS for the FM island with an adatom following the procedure found in Ref. 62, which was applied in the Kondo model with unpolarized bulk electrons. Such a method allows us to express the SR-LDOS in terms of the phase shifts due to the adatom scattering and the Fano effect. This latter is originated in the interference between the electron paths formed by the host conduction band and the Anderson impurity. We emphasize that the STM probe is not present in this section. Initially, we derive a formalism for finite T and later on we take the limit $T \rightarrow 0$. It is well known that

$$\rho^{\sigma}_{\rm LDOS}(\omega, R) = -\frac{1}{\pi}{\rm Im}\{\mathcal{G}_{\sigma}(\omega, R)\} \tag{23}$$

provides the SR-LDOS formula. The GF $\mathcal{G}_{\sigma}(\omega, R)$ is obtained from the Fourier transform of

$$\mathcal{G}_{\sigma}(\tau, R) = -\frac{i}{\hbar}\theta(\tau){\rm Tr}\{\varrho_{\rm FM}[\Psi_{R\sigma}(\tau), \Psi^{\dagger}_{R\sigma}(0)]_{+}\} \tag{24}$$

in time coordinate, where $\varrho_{\rm FM}$ and $[\ldots, \ldots]_{+}$ are the density matrix of the FM island Hamiltonian and the anticommutator between the operators given by Eq. (11) at different times, respectively.

In order to be explicit, we have to apply the equation of motion procedure (EOM) on Eq. (24) to demonstrate that $\mathcal{G}_{\sigma}(\omega, R)$ is coupled to other GFs as follows:

$$\mathcal{G}_{\sigma}(\omega, R) = g_{\sigma}(\omega, 0) + \tilde{g}_{\sigma}(\omega, R)\mathcal{T}_{\sigma}(\omega)\tilde{g}_{\sigma}(\omega, -R). \tag{25}$$

The first term

$$g_{\sigma}(\omega, R) = \frac{1}{N_{{\rm FM}\sigma}}\sum_{\vec{k}} \frac{e^{i\vec{k}.\vec{R}}}{\omega - \varepsilon_{k\sigma} + i\eta} \tag{26}$$

describes the bare GF for an uncorrelated electron state at the site $\vec{R}$, laterally displaced from the adatom, and

$$\tilde{g}_{\sigma}(\omega, R) = \frac{1}{N_{{\rm FM}\sigma}}\sum_{\vec{k}} \frac{\Gamma^2}{\Gamma^2 + \varepsilon^2_{k\sigma}} \frac{e^{i\vec{k}.\vec{R}}}{\omega - \varepsilon_{k\sigma} + i\eta} \tag{27}$$

is the correspondent one dressed by the nonlocal hybridization [Eq. (4)]. As a scattering center, the adatom defines a scattering amplitude

$$\mathcal{T}_{\sigma}(\omega) = \frac{\Delta}{\pi\rho_0}\mathcal{G}^{dd}_{\sigma}(\omega) \tag{28}$$

proportional to the GF $\mathcal{G}^{dd}_{\sigma}(\omega)$.

The emergence of Fano interference and Friedel oscillations in the system SR-LDOS is a result of the interplay between Eqs. (26) and (27). These effects can be elucidated by regrouping the terms in Eq. (25) in such a way to achieve the form

$$\rho^{\sigma}_{\rm LDOS}(\omega, R) = \rho_{{\rm FM}\sigma} + \pi\rho_0^2\left\{\left[A^2_{\sigma}(R) - q^2_{{\rm FM}\sigma}\right] \times {\rm Im}\{\mathcal{T}_{\sigma}(\omega)\} + 2A_{\sigma}(R) q_{{\rm FM}\sigma}{\rm Re}\{\mathcal{T}_{\sigma}(\omega)\}\right\}, \tag{29}$$

where Re means real part,

$$q_{{\rm FM}\sigma} = \frac{1}{\pi\rho_0}{\rm Re}\{\tilde{g}_{\sigma}(\omega, R)\} = \frac{\rho_{{\rm FM}\sigma}}{\rho_0} J_0(k_{F\sigma}R)\frac{\Gamma}{\Gamma^2 + \omega^2}\omega \tag{30}$$

represents the Fano parameter due to the adatom-island hybridization in the wide-band limit and characterized by spin-polarized Friedel oscillations in the zeroth-order Bessel function $J_0(k_{F\sigma}R)$. The spin-dependent Fermi wave numbers $k_{F\uparrow}$ and $k_{F\uparrow}$ are related to each other via

$$k_{F\uparrow} = \sqrt{\frac{1 - P}{1 + P}}k_{F\downarrow}, \tag{31}$$

deduced from Eqs. (3) and (6). The SR-LDOS also depends on the function

$$A_\sigma(R) = \frac{1}{\pi\rho_0}\mathrm{Im}\{\tilde{g}_\sigma(\omega,R)\} = \frac{\rho_{\mathrm{FM}\sigma}}{\rho_0}J_0(k_{F\sigma}R)\frac{\Gamma^2}{\Gamma^2+\omega^2} \tag{32}$$

that encloses spin-polarized Friedel oscillations for charge. Details of the method employed to derive Eq. (30) appear in Appendix B. We mention that to compare the SR-LDOS simulations of Sec. V to the experimental data measured in a Fe island with a Co adatom,[49] it is necessary to set the Fano parameter in Eq. (30) as a spinless ratio and equal to zero.

At low-temperature limit, the SR-LDOS is well described by Eq. (29) at the ground state. In such a region, it is possible to classify the SR-LDOS in terms of the spin-dependent phase shift $\delta_\sigma(\omega)$ for the conduction electrons due to the adatom scattering center. According to the results on the SIAM,[67] this characterization is obtained using the relation

$$\exp[2i\delta_\sigma(\omega)] = 1 - 2\pi\rho_0\frac{1}{N_{\mathrm{FM}\sigma}}\sum_{\vec{k}}\left(\frac{\Gamma^2}{\Gamma^2+\varepsilon_{k\sigma}^2}\right)^2\mathcal{T}_\sigma(\omega)i \times \delta(\omega-\varepsilon_{k\sigma}) \tag{33}$$

that correlates the phase shift $\delta_\sigma(\omega)$ to the real and imaginary parts of the scattering amplitude $\mathcal{T}_\sigma(\omega)$, given by Eq. (28), thus resulting in the formula

$$\tan\delta_\sigma(\omega) = \frac{\mathrm{Im}\{\mathcal{T}_\sigma(\omega)\}}{\mathrm{Re}\{\mathcal{T}_\sigma(\omega)\}}. \tag{34}$$

For the Fano interference, we define an analogous relation,[9–11] introducing the phase shift $\delta_{q_{\mathrm{FM}}}$ as

$$\tan\delta_{q_{\mathrm{FM}}} = -\frac{\mathrm{Re}\{\tilde{g}_\sigma(\omega,R)\}}{\mathrm{Im}\{\tilde{g}_\sigma(\omega,R)\}} = -\pi\rho_0\frac{q_{\mathrm{FM}\sigma}}{\mathrm{Im}\{\tilde{g}_\sigma(\omega,R)\}}, \tag{35}$$

in order to show that

$$\rho^\sigma_{\mathrm{LDOS}}(\omega,R) = \rho_{\mathrm{FM}\sigma}\left[1 - J_0^2(k_{F\sigma}R)\mathcal{F}_\sigma(\omega)\right] \tag{36}$$

becomes the expression for the system SR-LDOS and characterized by

$$\mathcal{F}_\sigma(\omega) = 1 - \frac{\cos^2[\delta_\sigma(\omega)-\delta_{q_{\mathrm{FM}}}]}{\cos^2\delta_{q_{\mathrm{FM}}}}, \tag{37}$$

exclusively expressed in terms of the adatom scattering and Fano phase shifts. The last formula is the main result of this section, and it represents the SR-LDOS of a metallic surface considered as a spin-polarized 2DEG coupled via a nonlocal hybridization to an adatom in the framework of the SIAM given by Eq. (2). In Sec. III B, we shall see that the STM spin-resolved conductance formula assumes identical structures to Eqs. (36) and (37), but with a redefined Fano parameter due to the probe presence.

B. Differential conductance and the SR-LDOS probed by the STM

In the low-temperature regime and for a STM probe not very close to the metallic sample, the spin-resolved and differential conductance of the STM device is proportional to an effective SR-LDOS. To derive this effective SR-LDOS, we have to implement the linear response theory treating the tunneling Hamiltonian in Eq. (10) as a perturbation, just to ensure the weak tunneling regime as verified in experimental conditions.[49] Taking these assumptions into account, we show that the spin-current follows the expression

$$I_\sigma = \frac{2e}{h}\pi\Gamma_w\int d\omega[n_F(\omega-e\phi)-n_F(\omega)]\tilde{\rho}^\sigma_{\mathrm{LDOS}}(\omega), \tag{38}$$

with $\Gamma_w = 2\pi|w|^2\rho_0$ as the parameter that hybridizes the system conduction bands, e the electron charge, ϕ the bias voltage, and

$$\tilde{\rho}^\sigma_{\mathrm{LDOS}}(\omega,R) = -\frac{1}{\pi}\mathrm{Im}\{\tilde{\mathcal{G}}_\sigma(\omega,R)\} \tag{39}$$

as the effective SR-LDOS probed by the STM device. Such density is calculated using the GF $\tilde{\mathcal{G}}_\sigma(\omega,R)$ obtained from the time Fourier transform of

$$\tilde{\mathcal{G}}_\sigma(\tau,R) = -\frac{i}{\hbar}\theta(\tau)\mathrm{Tr}\{\varrho_{\mathrm{FM}}[\tilde{\Psi}_{R\sigma}(\tau),\tilde{\Psi}^\dagger_{R\sigma}(0)]_+\}, \tag{40}$$

written in terms of the operator

$$\tilde{\Psi}_{R\sigma} = \Psi_{R\sigma} + (\pi\Delta\rho_0)^{1/2}q_R d_\sigma, \tag{41}$$

which describes the couplings between the probe and the island with the adatom, which depends on the new Fano parameter defined by

$$q_R = (\pi\Delta\rho_0)^{-1/2}(t_{dR}/w) = q_o\exp(-k_F R), \tag{42}$$

due to the interference between these additional conduction channels. To obtain the differential conductance $G_\sigma = \frac{\partial}{\partial\phi}I_\sigma$ for a given spin, we consider Eq. (38) and show that

$$G_\sigma = \frac{2e^2}{h}\pi\Gamma_w\int d\omega\left\{-\frac{\partial}{\partial\omega}n_F(\omega-e\phi)\right\}\tilde{\rho}^\sigma_{\mathrm{LDOS}}(\omega,R) \tag{43}$$

is the spin-resolved conductance for the STM device.

Note that the spin effects on the system conductance lie on the free density of states of the island in Eq. (6) and on the scattering amplitude $\mathcal{T}_\sigma(\omega)$ in Eq. (28) due to the adatom. Thus, we need to express Eq. (39) in terms of the adatom GF $\mathcal{G}^{dd}_\sigma(\omega)$ by employing the EOM procedure. This method leads to

$$\tilde{\mathcal{G}}_\sigma(\omega,R) = \mathcal{G}_\sigma(\omega,R) + \pi\Delta\rho_0 q_R^2\mathcal{G}^{dd}_\sigma(\omega) + (\pi\Delta\rho_0)^{1/2}q_R \times \mathcal{G}^{\Psi d}_\sigma(\omega,R) + (\pi\Delta\rho_0)^{1/2}q_R\mathcal{G}^{d\Psi}_\sigma(\omega,R), \tag{44}$$

and displays that such GF is linked to Eq. (25) for the site $\vec{R}$ of the island and simultaneously to

$$\mathcal{G}^{\Psi d}_\sigma(\omega,R) = (\pi\Delta\rho_0)^{1/2}[q_{\mathrm{FM}\sigma} - iA_\sigma(R)]\mathcal{G}^{dd}_\sigma(\omega) \tag{45}$$

and $\mathcal{G}^{d\Psi}_\sigma(\omega,R)$, where the former expression is obtained from the time Fourier transformation of

$$\mathcal{G}^{\Psi d}_\sigma(\tau) = -\frac{i}{\hbar}\theta(\tau)\mathrm{Tr}\{\varrho_{\mathrm{FM}}[\Psi_{R\sigma}(\tau),d^\dagger_\sigma(0)]_+\}, \tag{46}$$

which is also equal to $\mathcal{G}^{\Psi d}_\sigma(\omega,R)$. Thus, replacing Eqs. (28), (44), and

$$-\frac{1}{\pi}\mathrm{Im}\{\mathcal{G}^{d\Psi}_\sigma(\omega,R)\} = \left(\frac{\Delta\rho_0}{\pi}\right)^{1/2}\{A_\sigma(R)\mathrm{Re}\{\mathcal{G}^{dd}_\sigma(\omega)\} - q_{\mathrm{FM}\sigma}\mathrm{Im}\{\mathcal{G}^{dd}_\sigma(\omega)\}\} \tag{47}$$

into Eq. (39), we find that

$$\tilde{\rho}^{\sigma}_{\mathrm{LDOS}}(\omega,R) = \rho_{\mathrm{FM}\sigma} + \pi\rho_0^2\{(A^2_{\sigma}(R) - q^2_{R\sigma}) \times \mathrm{Im}\{\mathcal{T}_{\sigma}(\omega)\} + 2A_{\sigma}(R)q_{R\sigma}\mathrm{Re}\{\mathcal{T}_{\sigma}(\omega)\}\} \tag{48}$$

obeys Eq. (29) for the SR-LDOS in the case of an absent STM probe, but with an effective Fano parameter

$$q_{R\sigma} = q_{\mathrm{FM}\sigma} + q_R, \tag{49}$$

which takes into account an intrinsic Fano interference ($q_{\mathrm{FM}\sigma}$) due to the adatom-island coupling represented by the first term and an extrinsic one (q_R) as a result of the STM probe hybridized with both adatom and the metallic surface, enclosed by the second part. We pointed out that for $T \ll T_K$, the spin-resolved conductance in Eq. (43) becomes directly proportional to the effective SR-LDOS evaluated at the energy $e\phi$. To show that, we use the Dirac delta distribution expressed by the minus derivative of the Fermi function in Eq. (43), which eliminates the integration over energy and gives

$$G_{\sigma} = \frac{2e^2}{h}\pi\Gamma_w\tilde{\rho}^{\sigma}_{\mathrm{LDOS}}(e\phi). \tag{50}$$

This result means that the effective SR-LDOS is a fairly representative function for the spin-resolved conductance of the system, which favors us to apply the zero-temperature formalism of phase shifts discussed in Sec. III A by introducing

$$\tan\delta_{q_{R\sigma}} = -\frac{q_{R\sigma}}{A_{\sigma}(R)} \tag{51}$$

as the total Fano phase shift. By combining it with Eq. (34) for the scattering amplitude $\mathcal{T}_{\sigma}(\omega)$, it is possible to derive

$$\tilde{\rho}^{\sigma}_{\mathrm{LDOS}}(\omega,R) = \rho_{\mathrm{FM}\sigma}\left[1 - J_0^2(k_{F\sigma}R)\tilde{\mathcal{F}}_{\sigma}(\omega,R)\right] \tag{52}$$

and

$$\tilde{\mathcal{F}}_{\sigma}(\omega,R) = 1 - \frac{\cos^2[\delta_{\sigma}(\omega) - \delta_{q_{R\sigma}}]}{\cos^2\delta_{q_{R\sigma}}} \tag{53}$$

as expressions that represent the effective SR-LDOS probed by the STM. The latter contains two sources for Fano effect: the first concerns the Fano interference between the traveling electrons through the host conduction band that can "visit" the adatom site and go back to it, and those that do not perform such a "visit."Additionally, the second process is composed by the couplings of the probe with the island and the adatom. It also has the scattering of the traveling electrons due to the side-coupled adatom, which in certain conditions leads to the Kondo effect. We also remark that the phase shift $\delta_{\sigma}(\omega)$ given by Eq. (34) is obtained in this work employing the atomic approach.

From Eq. (52), we are able to determine the following occupation number:

$$n^{\sigma}_{\mathrm{LDOS}} = \int_{-\infty}^{+\infty} d\omega\,\tilde{\rho}^{\sigma}_{\mathrm{LDOS}}(\omega,R=0)n_F(\omega). \tag{54}$$

As we shall see, this formula will guide us to better understand the results of Sec. IV.

IV. RESULTS

Here, we present the results obtained via the formulation developed in the previous section. We employ a set of parameters that define the Kondo regime: $E_d = -10.0\Delta$ and $V = 12.0\Delta$, where $\Delta = 0.01D_0$ ($D_0 = 1.0$). We will basically compare two regimes of q_0 value. The large q_0 limit we call *peak limit* due to the formation of a Kondo peak in the LDOS. The other regime, corresponding to small and intermediate values of q_0, we call *dip limit* since the LDOS presents a dip around the Fermi level.

It is necessary to mention that the SR-LDOS formula derived in the previous section is valid for zero temperature. On the other hand, the numerical procedure of the atomic approach is well established for $T \ll T_K$ but still finite T. So, we consider a very low temperature $T = 0.001\Delta$ to allow the combination of both procedures. To investigate the spatial behaviors of the Fano factor and the LDOS, we define a dimensionless parameter $k_{F\downarrow}R = k_FR$ to represent the STM probe-adatom lateral distance in Fig. 1.

A. Intrinsic Fano parameter

Here, we look with some more detail at the spatial dependence of the intrinsic Fano factor $q_{\mathrm{FM}\sigma}$. Figure 2(a) shows $q_{\mathrm{FM}\sigma}$ against k_FR for $P = 0.3$, $\omega = 0.02D_0$, and $\Gamma = 0.1\omega$. Interestingly, this Fano factor reveals spin-polarized Friedel oscillations. These oscillations exhibit enhanced amplitudes for the spin-up channel and a phase shifted pattern in relation to the spin-down component due to the spin-dependent Fermi wave number [Eq. (31)]. This phase shift yields irregular oscillations in the total Fano parameter $q_{\mathrm{FM}} = q_{\mathrm{FM}\uparrow} + q_{\mathrm{FM}\downarrow}$ [Figs. 2(a) and 2(b)].

In Fig. 2(b), we can also observe by changing from $\Gamma = 10\omega$ to 40ω that the spin-polarized Fano parameters approach to zero, exhibiting flattened oscillations as a function of k_FR. For large enough Γ, we have $q_{\mathrm{FM}\sigma} \approx 0$. Since the present atomic approach is valid only for constant $V_{dk\sigma}$, which is obtained for large Γ (local coupling), we will restrict our analysis to negligible $q_{\mathrm{FM}\sigma}$ values. In particular, for a perfect local coupling configuration, settled by the condition $q_{\mathrm{FM}\sigma} = 0$ in Eq. (30), we can conclude according to Eq. (49) that the Fano parameter q_o induced by the STM probe is the only one that rules the Fano interference in the system. In Secs. IV B and IV C, we discuss the possible interference limits for q_o in the local coupling regime, where the atomic approach is applicable.

B. SR-LDOS in the peak limit ($q_o = 100$)

Figures 3(a)–3(c) show the SR-LDOS and total LDOS for increasing polarization degree of the host. In the unpolarized case $P = 0$ (not shown), we have the well-known twofold-degenerate Kondo peak as in the SET.[2,3] However, for increasing P, this degeneracy is broken and the Kondo peak splits into two peaks. While the corresponding spin-up peak presents a slight shift for increasing P, the spin-down one remains pinned around the host Fermi level. Additionally, the widths of these peaks show opposite behaviors. While the up-peak broadens, the down-peak shrinks as P enlarges. In the insets we present with more detail the SR-LDOS around

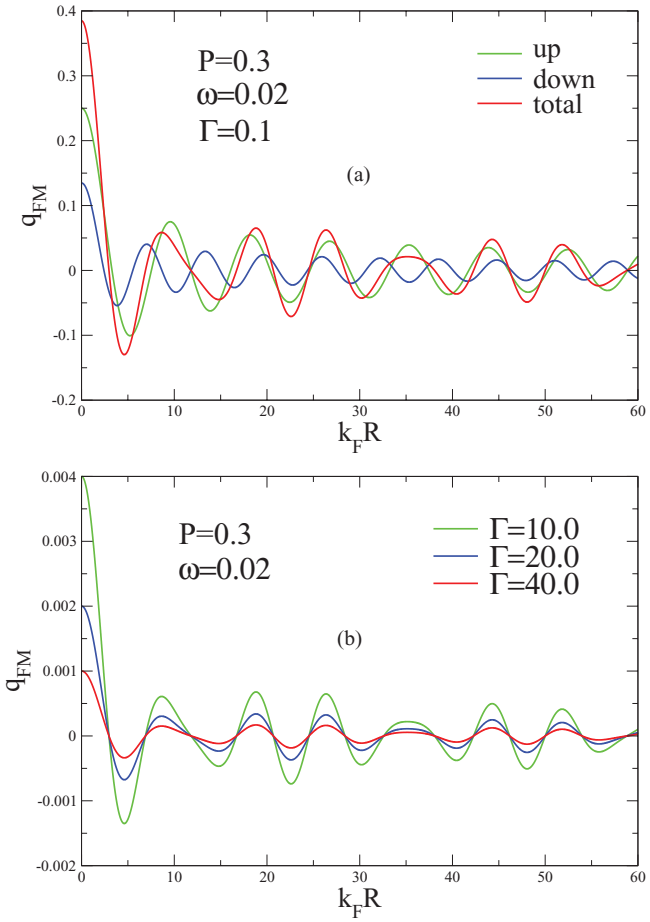

FIG. 2. (Color online) (a) Spin-polarized Fano factors $q_{\mathrm{FM}\sigma}$ for $\Gamma = 0.1$ and (b) the sum $q_{\mathrm{FM}} = q_{\mathrm{FM}\uparrow} + q_{\mathrm{FM}\downarrow}$ for $\Gamma = 10.0$, $\Gamma = 20.0$, and $\Gamma = 40.0$ in units of ω as a function of the dimensionless parameter $k_F R$.

the Fermi level, where we can see more clearly the spin splitting of the Kondo resonance.

Thus, it is valid to mention that our spin splitting resembles the work of Qi *et al.*[36] for a spin current injected in a nonmagnetic conductor with a Kondo adatom. In this work, it is possible to note a tendency of a pinning for one spin component of the Kondo peak. Kondo peak splitting was also observed in a QD system hybridized to ferromagnetic reservoirs[37] and in the presence of spin flip.[35]

In the experimental point of view, the spin splitting of the Kondo resonance has already been observed in systems of QDs coupled to ferromagnetic reservoirs[45] and in a carbon nanotube QD interacting with a magnetic particle.[50] Observe that for $P = 0.2$ and 0.5, it is not possible to resolve the spin splitting of the Kondo peak in the total LDOS. Experimentally, nonresolved Kondo peak splitting can also occur.[47] Although the STM experiments are in general restricted to energies around the host Fermi level, here we show the SR-LDOS for a wider energy window in order to see the polarization effects on the adatom level E_d, as displayed in Fig. 3.

The analysis of the non-Zeeman splitting in the full LDOS for different STM probe positions is presented in Fig. 4 for $P = 0.5$. We see that the LDOS profile becomes flatter for large enough values of the dimensionless parameter $k_F R$, thus

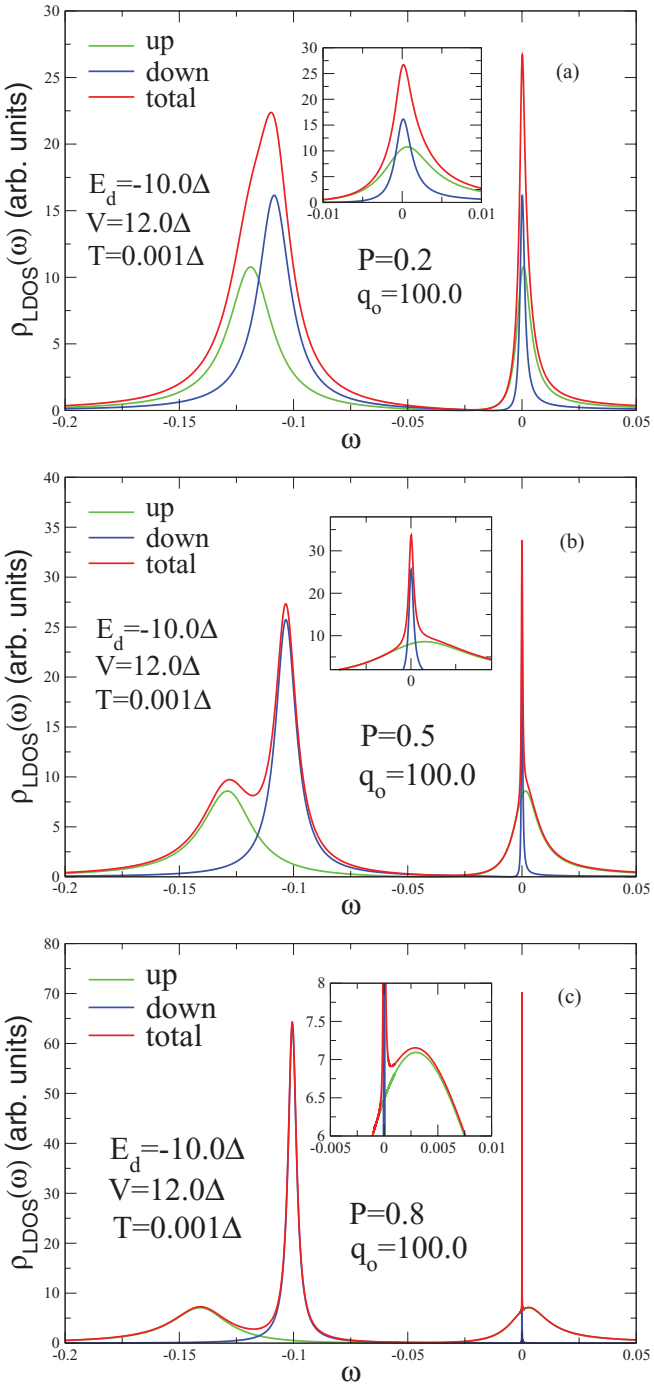

FIG. 3. (Color online) Spin-resolved local density of states (SR-LDOS) at $R = 0$, in arbitrary units (arb. units), as a function of the energy ω for increasing P value: (a) $P = 0.2$, (b) $P = 0.5$, and (c) $P = 0.8$. In the insets, we show the SR-LDOS around the host Fermi level, where we can see the Kondo peak splitting with the pinning of the spin-down component. We also observe that as P increases, the spin-down resonance shrinks.

revealing a crossover from the *peak limit* at $R = 0$ to the background value represented by the host free density of states [Eq. (8)].

We end this section presenting Fig. 5, where the dependence of the spin splitting of the Kondo peak ΔE as a function of the host polarization P can be observed. Note that ΔE displays a

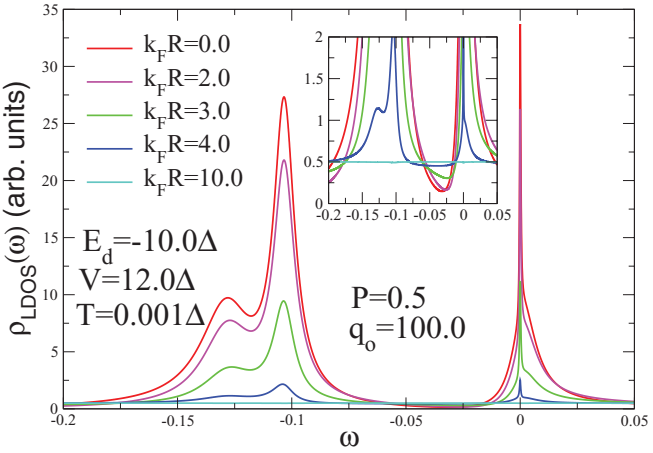

FIG. 4. (Color online) Local density of states (LDOS), in arbitrary units (arb. units), as a function of the energy ω for different $k_F R$ values. In the inset, we present the LDOS in detail.

nonlinear behavior as P increases. This nonlinearity was also found by Qi *et al.*.[36]

C. SR-LDOS in the dip limit ($q_0 \leqslant 1$)

In contrast to the $q_0 = 100$ case previously analyzed in the *peak limit*, here we discuss the $q_0 \leqslant 1$ regime. This corresponds to a direct STM probe and host surface tunneling being dominant. In this situation, the system reduces to an adatom side coupled to the FM island as represented in Fig. 1, which is equivalent to the T-shaped QD device.[7] For small Fano factors ($q_0 = 0.01$), the LDOS exhibits antiresonances (dips) instead of resonances, as we can see in Fig. 6(a). This happens in such a way that the antiresonance in the up SR-LDOS channel disappears for high enough polarization as seen in the inset of Fig. 6(a). On the other hand, the dip of the down component shrinks as P increases. The width of this antiresonance lowers two orders of magnitude when we change the polarization from $P = 0.2$ to 0.8. So, we can conclude that the polarization induces a continuous second-order insulator-metal transition in the system. As the polarization grows from $P = 0$ to 0.8, the up SR-LDOS

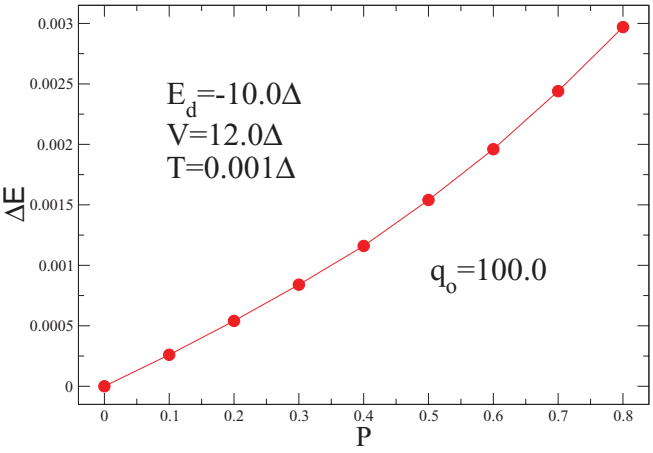

FIG. 5. (Color online) Kondo peak splitting ΔE in units of D_0, as a function of the host polarization P.

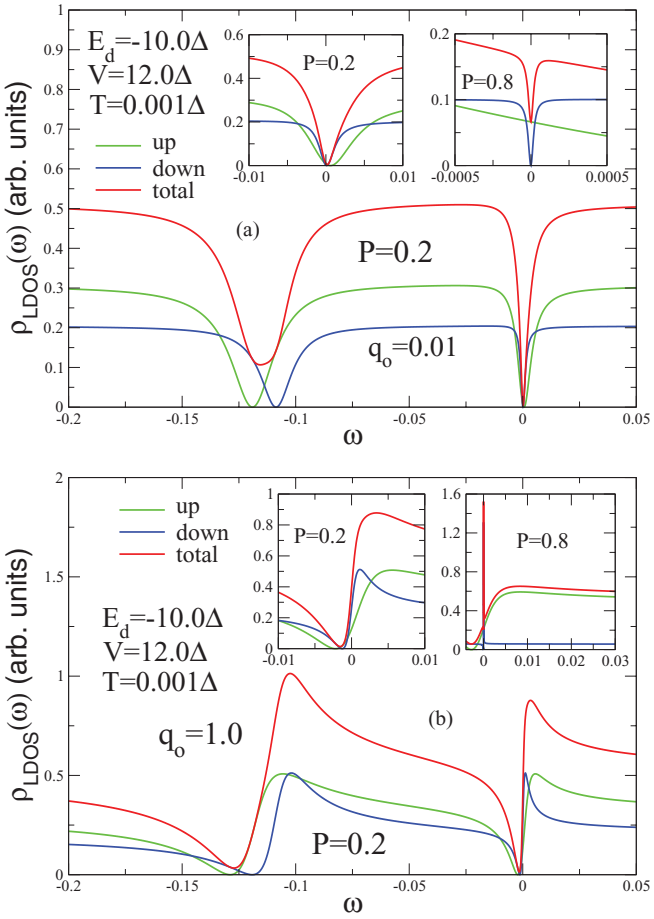

FIG. 6. (Color online) Spin-resolved local density of states (SR-LDOS) at $R = 0$, in arbitrary units (arb. units), as a function of the energy ω. In the full curve, we show the local density of states (LDOS). In the insets, we present the SR-LDOS and the LDOS in the vicinity of the Fermi energy $\omega \simeq \varepsilon_F = 0$. For $P = 0.2$, there is a Fano-Kondo structure in the LDOS profile, but for $P = 0.8$ an enhanced Kondo peak appears in the spin-down channel.

component becomes continuously flat, generating a finite SR-LDOS in the vicinity of the Fermi energy $\omega \simeq \varepsilon_F = 0$. At the same time, the down SR-LDOS component shrinks, closing the total LDOS gap, as indicated in the inset of Fig. 6(a) for $P = 0.8$.

The last cases in the *dip limit* we investigate correspond to $q_o = 1$, $P = 0.2$, and $P = 0.8$ as presented in Fig. 6(b). For the low polarization $P = 0.2$, the Fano interference is robust, presenting the coexistence of a structure composed by dips and peaks (Fano line shape). However, for the large polarization $P = 0.8$, the Kondo peak in the adatom GF prevails in the spin-down channel and suppresses the destructive interference. This feature appears in the insets of Fig. 6(b).

The simulations presented resemble experimental results found in ferromagnetic contacts as in the Calvo *et al.* work[47] [see their Fig. 1(c)] and adatoms systems discussed by Néel *et al.*[34] [see their Fig. 1(b)]. In the former experiment, depending on the electrodes composition coupled to the contact, the energy profile of the conductance displays patterns without resolved spin splitting. This behavior is related to the cases of small and intermediate values of the Fano parameter,

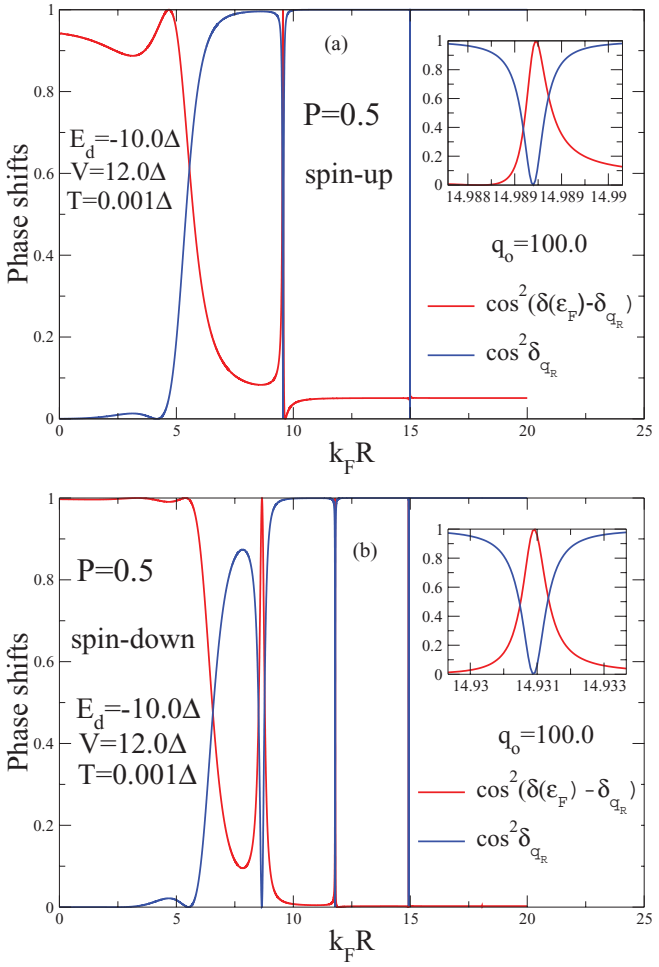

FIG. 7. (Color online) Analysis of the system phase shift structure evaluated at the host Fermi level. Plots of $\cos^2[\delta_\sigma(\varepsilon_F) - \delta_{q_{R\sigma}}]$ and $\cos^2 \delta_{q_{R\sigma}}$ as a function of the dimensionless parameter $k_F R$ for both spin components. In the inset, we show the resonance and antiresonance features at $k_F R \simeq 15.0$.

which were obtained with Fe and Co contacts, respectively. For the second experiment, spin-polarized STM probes made by Fe or W were employed on a Co adatom deposited on a Cu(111) surface. In particular, in this case no resolved spin splitting was verified, which corresponds to the limit of small Fano factor. These setups can be reproduced in our simulations considering intermediate polarizations.

D. Phase shifts and occupation numbers

In Sec. III B, we show that the SR-LDOS can be expressed in terms of the phase shifts $\delta_\sigma(\omega)$ and $\delta_{q_{R\sigma}}$. Here, we explore the quantities $\cos^2 \delta_{q_{R\sigma}}$ and $\cos^2[\delta_\sigma(\omega) - \delta_{q_{R\sigma}}]$ in order to gain further insight about the spin splitting and Kondo peak pinning found in the SR-LDOS. In Fig. 7, we present these two functions against $k_F R$ for both spin components, where the numerical parameters are indicated in the plots. The main distinction between the up and down curves can be observed in the range $0 < k_F R < 5.0$ where $\cos^2[\delta_\sigma(\varepsilon_F) - \delta_{q_{R\sigma}}] \approx 1$ for spin down, while it stays below 1 for spin up. In particular, for $k_F R \to 0$, we find $\cos^2(\delta_{q_{R\sigma}}) \to 0$, which means that $\delta_{q_{R\sigma}} \to \pi/2$. Consequently, $\cos^2[\delta_\sigma(\varepsilon_F) - \delta_{q_{R\sigma}}] \to \sin^2[\delta_\sigma(\varepsilon_F)]$. On the other hand, according to Friedel sum rule [Eq. (21)], we have $\delta_\sigma(\varepsilon_F) = \pi n_{d,\sigma}$. This implies that $n_{d,\downarrow} \to 0.5$ while $n_{d,\uparrow}$ stays below 0.5. The fact that $n_{d,\downarrow}$ remains close to 0.5 results in the pinning of the spin-down component of the Kondo resonance. For increasing $k_F R$, the curves obtained from Eq. (51) display a series of peaks and dips due to the interplay between the exponential decay in Eq. (12) and the Friedel oscillations.

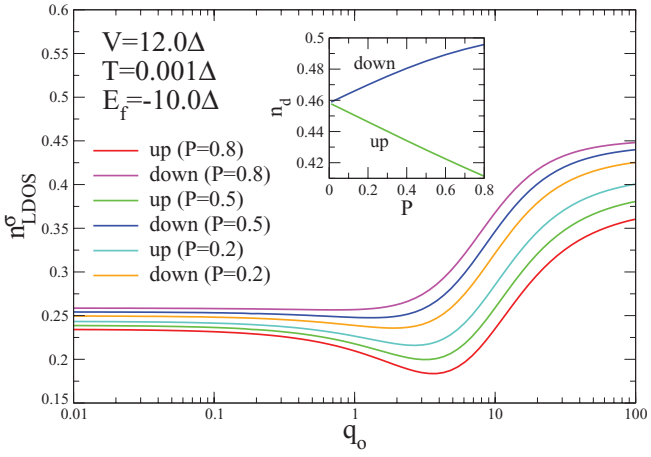

FIG. 8. (Color online) Occupation number n^σ_{LDOS} of Eq. (54) as a function of the Fano parameter q_o and with different values for the spin polarization P of the host. In the inset, we present $n_{d,\sigma}$ against P.

To complement the analysis on the emergence of the Kondo peak pinning, we present Fig. 8. In such a figure, we plot the occupation number n^σ_{LDOS} of Eq. (54) as a function of the Fano factor q_0 for differing spin polarizations P. This gives also the same tendency of $n_{d,\uparrow}$ and $n_{d,\downarrow}$ since both n^σ_{LDOS} and $n_{d,\sigma}$ should preserve some proportionality. In the large q_0 limit, $n^\downarrow_{\mathrm{LDOS}}$ approaches to 0.45, while $n^\uparrow_{\mathrm{LDOS}}$ moves to lower values as P increases. This corroborates the pinning of the spin-down Kondo resonance. Note that the Friedel sum rule given by Eq. (21) ensures the pinning of the Kondo peak in the down channel and the displacement of the up peak via the inequality $n_{d,\uparrow} < n_{d,\downarrow} \approx 0.5$. In the inset of Fig. 8, the plots of $n_{d,\uparrow}$ and $n_{d,\downarrow}$ against P confirm this inequality. Such occupations indicate that there is a net magnetic moment at the adatom partially screened by the conduction electrons, where the lack of spin-down conduction electrons is not able to blind the spin-up component of the impurity, thus avoiding a formation of a defined Kondo peak in that channel. On the other hand, the excess of spin-up conduction electrons yields to a Kondo peak in the down component of the adatom DOS. We can conclude that there is no abrupt breakdown of the Kondo effect, but a crossover from the ordinary Kondo effect to a situation where the Kondo effect is gradually suppressed.

V. ANALYSIS OF SOME EXPERIMENTAL RESULTS

In this section, we successfully apply the present developed formulation to reproduce recent experimental findings on a single Kondo adatom coupled to a magnetic cluster. To our best knowledge, the first experimental work that explores

Kondo adatom on a ferromagnetic host was recently done by Kawahara *et al.*,[49] which used an unpolarized STM probe on top of a Fe island with a Co adatom. They observed that, depending on the adsorption site of the Co atom, a spin splitting of a Fano-Kondo dip is induced by the spin polarization of the island, and can be explained by a double Fano antiresonance in a single-particle picture.

As pointed out in Ref. 49, there are two competing mechanisms that can result or not in the Kondo effect. The first one is the antiferromagnetic exchange interaction between the Co adatom and the itinerant sp island electrons. The second one is the exchange interaction due to the direct $d-d$ ferromagnetic interaction of the Co adatom and the Fe atoms of the magnetic substrate. Our formulation only can be applied to this system if the antiferromagnetic interaction dominates over the direct ferromagnetic correlation. These competing processes appear in Ref. 49 as an assumption, but further experimental and theoretical investigations are necessary to better understand the dominant mechanism.

There are some related experimental results, supported by first-principles calculations of Calvo *et al.*,[47] in related systems. They found the existence of a Kondo peak in ferromagnetic atomic contacts hybridized with electrodes (both built by Fe, Ni, and Co), differently from those found in the bulk limit. In nanoscale, the electrons at the surfaces of these junctions experience interactions where the antiferromagnetic coupling overcomes the ferromagnetic correlations. In such setups, the nanocontacts play the role of the Co adatom used in the work of Kawahara *et al.*. Thus, our model in its present form does not support the opposite case characterized by strong ferromagnetic correlations, which are usually modeled by a Heisenberg-type interaction. For an enhanced antiferromagnetic coupling between the sp electrons and the adatom, the picture of a spin-polarized electrons gas as discussed by Calvo *et al.*[47] can be employed to describe a ferromagnetic metallic sample with a Kondo impurity. Additionally, we would like to remark that Kondo adatoms and some QD systems indeed have a spin $S > 1/2$, which can be detectable by a magnetic anisotropy signature.[23,53,55] In these cases, a multiorbital Anderson Hamiltonian could offer a more detailed modeling[22,51] and improve the accuracy of this work.

However, we changed the localized adatom level E_d in all the relevant parameter ranges of the SIAM in order to better reproduce the line shape of the work of Kawahara *et al.* The optimized values are $E_d = -3.0\Delta$ and $q_0 = 0.01$, which characterize the intermediate valence regime of the system.

It is clear from Fig. 9 that the resolved LDOS double-dip structure is originated from the splitting of the up- and down-spin components. To show the evolution of the double structure at $\omega \simeq \varepsilon_F = 0$ from the Kondo peak to the intermediate valence regime, we present in the inset (I) of Fig. 9 the splitting of the Fano-Kondo dip for $E_d = -10\Delta$, whereas in the inset (II) we present the correspondent case in the same energy range, but for the intermediate valence situation, with $E_d = -3\Delta$. In this last regime, the spin-down channel is also pinned at $\omega \simeq \varepsilon_F = 0$, and the spin up is displaced from it. Note that, for this set of parameters, the Fano-Kondo dip splitting is resolved in the LDOS. The inset (II) displays more precisely the spin-polarized antiresonances analogous to those

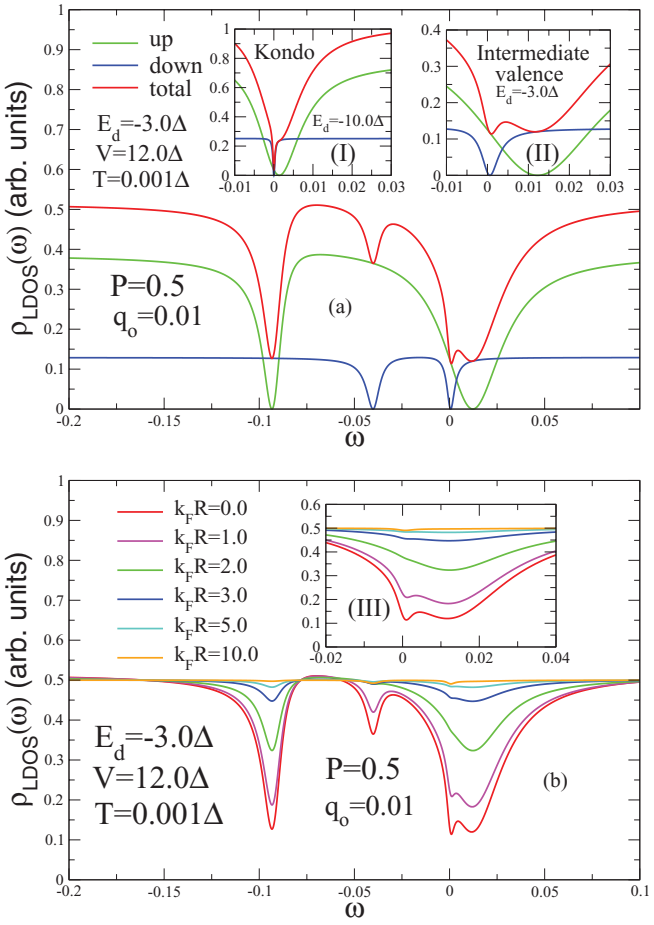

FIG. 9. (Color online) Spin-resolved local density of states (SR-LDOS) at $R = 0$, in arbitrary units (arb. units), as a function of the energy ω. In the full curve, we represent the total density of states (LDOS). (a) In the inset (I), we present the splitting of the Fano-Kondo dip in the Kondo peak region for $E_d = -10\Delta$, whereas in the inset (II) we perform the same analysis for the intermediate valence case, using $E_d = -3\Delta$. In the inset (III), we present the suppression of the double Fano-Kondo dip structure as a function of $k_F R$.

observed in Fig. 1(b) of Ref. 49. In Fig. 9(b), we present the SR-LDOS as a function of the energy ω for different lateral STM-probe distances. As $k_F R$ increases, the Fano-Kondo dips disappear gradually, and for $k_F R \simeq 10.0$, we recover the uncorrelated conduction band [see the inset (III)]. Similar behavior is observed in Fig. 3 of Ref. 49.

VI. CONCLUSIONS

We studied the spin-resolved local density of states (SR-LDOS) of a system composed of a Kondo adatom on a spin-polarized two-dimensional electron gas in the presence of an unpolarized STM probe. We derived the SR-LDOS expression in both the presence and absence of the STM probe. Our expression to the SR-LDOS in terms of phase shifts is general and independent of the method employed to calculate the local adatom GF. To determine this GF, we used the atomic approach in the limit of infinite U. The coupling

parameter between adatom and host is assumed constant (local coupling).

We were able to study the SR-LDOS in all the interference regimes, varying the Fano factor q_o. The main effect of the polarization was the tendency of one spin peak ($q_0 = 100$) or dip ($q_0 = 0.01$, $q_0 = 1$) in the SR-LDOS to remain pinned around the host Fermi level as the polarization P increases. In contrast, the other spin peak or dip is shifted and loses amplitude as P increases. This contrasts to the usual behavior in the presence of a magnetic field, where the Kondo resonance is symmetrically spin split and destroyed as the magnetic field increases, while here it is enhanced in one channel (down) and destroyed in the other (up).

Our simulations are in close agreement with recent experimental results on adatom coupled to a ferromagnetic island.[49] The present system is a potential candidate to promote the Kondo peak splitting without application of huge magnetic fields necessary for adatom systems characterized by a large T_K. In particular, for the Fano factor $q_o = 0.01$, we observed a continuous second-order insulator-metal transition driven by the polarization as presented in Fig. 6(a). Finally, our model was able to describe qualitatively several experimental results.[34,45,47,49,50]

ACKNOWLEDGMENT

This work was supported by the Brazilian agencies CNPq, CAPES, and FAPEMIG.

APPENDIX A: THE ATOMIC GF FOR THE KONDO ADATOM

In this Appendix, we present expressions employed in the spin-dependent GF for the Kondo adatom considering the SIAM in the atomic version given by Eq. (13) of Sec. II B. To obtain the atomic GF, we use Zubarev's notation[69]

$$\mathcal{G}^{dd}_{\mathrm{at},\sigma}(\omega) = e^{\beta\Omega}\sum_{jj'}(e^{-\beta E_j} + e^{-\beta E_{j'}}) \times \frac{|\langle j'|\, X_{d,\sigma\sigma}\, |j\rangle|^2}{\omega - (E_j - E_{j'})}, \tag{A1}$$

where $\beta = 1/k_BT$ with k_B as the Boltzmann constant, T is the system temperature, and Ω is the thermodynamical potential. The eigenvalues E_j and eigenvectors $|j\rangle$ correspond to the complete solution of the SIAM Hamiltonian. The final result is the following:

$$\mathcal{G}^{dd}_{\mathrm{at},\sigma}(\omega) = e^{\beta\Omega}\sum_{i=1}^{8}\frac{m_{i\sigma}}{\omega - u_{i\sigma}}, \tag{A2}$$

where the poles and the residues are

$$\begin{aligned}
u_{1\sigma} &= E_{3\sigma} - E_{1\sigma} = E_{8\sigma} - E_{5\sigma} = E_{7\sigma} - E_{4\sigma} = \tfrac{1}{2}(\varepsilon_{dk\sigma} - \delta_\sigma),\\
u_{2\sigma} &= E_{5\sigma} - E_{1\sigma} = E_{8\sigma} - E_{3\sigma} = E_{7\sigma} - E_{2\sigma} = \tfrac{1}{2}(\varepsilon_{dk\sigma} + \delta_\sigma),\\
u_{3\sigma} &= E_{12\sigma} - E_{10\sigma} = \tfrac{1}{2}(\varepsilon_{dk\sigma} - \delta'_\sigma),\\
u_{4\sigma} &= E_{12\sigma} - E_{9\sigma} = \tfrac{1}{2}(\varepsilon_{dk\sigma} + \delta'_\sigma),\\
u_{5\sigma} &= E_{9\sigma} - E_{2\sigma} = \varepsilon_{k\sigma} - \tfrac{1}{2}(\delta'_\sigma - \delta_\sigma),\\
u_{6\sigma} &= E_{10\sigma} - E_{2\sigma} = \varepsilon_{k\sigma} + \tfrac{1}{2}(\delta'_\sigma + \delta_\sigma),\\
u_{7\sigma} &= E_{9\sigma} - E_{4\sigma} = \varepsilon_{k\sigma} - \tfrac{1}{2}(\delta'_\sigma + \delta_\sigma),\\
u_{8\sigma} &= E_{10\sigma} - E_{4\sigma} = \varepsilon_{k\sigma} + \tfrac{1}{2}(\delta'_\sigma - \delta_\sigma)
\end{aligned} \tag{A3}$$

and

$$\begin{aligned}
m_{1\sigma} &= c^2_{1\sigma}\left[1 + e^{-\frac{1}{2}\beta(\varepsilon_{dk\sigma} - \delta_\sigma)} + \frac{3}{2}e^{-\frac{1}{2}\beta(\varepsilon_{dk\sigma} + \delta_\sigma)} + \frac{3}{2}e^{-\beta\varepsilon_{dk\sigma}}\right],\\
m_{2\sigma} &= s^2_{1\sigma}\left[1 + e^{-\frac{1}{2}\beta(\varepsilon_{dk\sigma} + \delta_\sigma)} + \frac{3}{2}e^{-\frac{1}{2}\beta(\varepsilon_{dk\sigma} - \delta_\sigma)} + \frac{3}{2}e^{-\beta\varepsilon_{dk\sigma}}\right],\\
m_{3\sigma} &= c^2_{2\sigma}\left[e^{-\frac{1}{2}\beta(\epsilon_d + 3\varepsilon_{k\sigma} + \delta'_\sigma)} + e^{-\frac{1}{2}\beta(\epsilon_d + 2\varepsilon_{k\sigma})}\right],\\
m_{4\sigma} &= s^2_{2\sigma}\left[e^{-\frac{1}{2}\beta(\epsilon_d + 3\varepsilon_{k\sigma} - \delta'_\sigma)} + e^{-\frac{1}{2}\beta(\epsilon_d + 2\varepsilon_{k\sigma})}\right],\\
m_{5\sigma} &= \frac{1}{2}s^2_{1\sigma}c^2_{2\sigma}\left[e^{-\frac{1}{2}\beta(\varepsilon_{dk\sigma} - \delta_\sigma)} + e^{-\frac{1}{2}\beta(\epsilon_d + 3\varepsilon_{k\sigma} - \delta'_\sigma)}\right],\\
m_{6\sigma} &= \frac{1}{2}s^2_{1\sigma}s^2_{2\sigma}\left[e^{-\frac{1}{2}\beta(\varepsilon_{dk\sigma} - \delta_\sigma)} + e^{-\frac{1}{2}\beta(\epsilon_d + 3\varepsilon_{k\sigma} + \delta'_\sigma)}\right],\\
m_{7\sigma} &= \frac{1}{2}c^2_{1\sigma}\, c^2_{2\sigma}\left[e^{-\frac{1}{2}\beta(\varepsilon_{dk\sigma} + \delta_\sigma)} + e^{-\frac{1}{2}\beta(\epsilon_d + 3\varepsilon_{k\sigma} - \delta'_\sigma)}\right],\\
m_{8\sigma} &= \frac{c^2_{1\sigma}s^2_{2\sigma}}{2}\left[e^{-\frac{\beta(\varepsilon_{dk\sigma} + \delta_\sigma)}{2}} + e^{-\frac{\beta(\epsilon_d + 3\varepsilon_{k\sigma} + \delta'_\sigma)}{2}}\right],
\end{aligned} \tag{A4}$$

respectively, which are defined in terms of

$$\begin{aligned}
\epsilon_d &= E_d - \varepsilon_F, \quad \epsilon_{k\sigma} = \varepsilon_{k\sigma} - \varepsilon_F,\\
s_{1\sigma} &= \sin\phi_\sigma, \quad c_{1\sigma} = \cos\phi_\sigma, \quad s_{2\sigma} = \sin\Lambda_\sigma,\\
c_{2\sigma} &= \cos\Lambda_\sigma, \quad \epsilon_d + \varepsilon_{k\sigma} = \varepsilon_{dk\sigma},\\
\delta_\sigma &= [(\varepsilon_{k\sigma} - \epsilon_d)^2 + 4V^2]^{1/2}, \quad \delta'_\sigma = [(\varepsilon_{k\sigma} - \epsilon_d)^2 + 8V^2]^{1/2},
\end{aligned} \tag{A5}$$

with ε_F being the Fermi energy and

$$\tan\phi_\sigma = \frac{2V}{\varepsilon_{k\sigma} - \epsilon_d + \delta_\sigma}, \quad \tan\Lambda_\sigma = \frac{2\sqrt{2}V}{\varepsilon_{k\sigma} - \epsilon_d + \delta'_\sigma}. \tag{A6}$$

APPENDIX B: FANO FACTOR FOR THE FM HOST

In order to determine the Fano factor given by Eq. (30) in Sec. III A due to the adatom-host coupling, we extend the procedure proposed for unpolarized bulk electrons[62] to conduction states of a FM surface. To that end, we perform the calculation assuming the wide-band limit conditions $\omega \ll D_\sigma$ and $\Gamma \ll D_\sigma$ in the advanced GF

$$\tilde{G}_\sigma(\omega, R) = \frac{1}{N_{\mathrm{FM}\sigma}}\sum_{\vec{k}}\frac{\Gamma^2}{\Gamma^2 + \varepsilon^2_{k\sigma}}\frac{e^{i\vec{k}.\vec{R}}}{\omega - \varepsilon_{k\sigma} - i\eta}, \tag{B1}$$

with $\eta \to 0^+$, which allows us, in combination with Eq. (32), to establish the following equalities:

$$\mathrm{Re}\{\tilde{G}_\sigma(\omega, R)\} = \mathrm{Re}\{\tilde{g}_\sigma(\omega, R)\} \tag{B2}$$

and

$$\mathrm{Im}\{\tilde{G}_\sigma(\omega, R)\} = -\mathrm{Im}\{\tilde{g}_\sigma(\omega, R)\} = \pi\rho_0 A_\sigma(R). \tag{B3}$$

Considering

$$J_0(kR) = \frac{1}{2\pi}\int_0^{2\pi}\exp[ikR\cos\theta_k]d\theta_k \tag{B4}$$

as the angular representation for the zeroth-order Bessel function in Eq. (32), and according to Eqs. (30) and (B2), the Fano factor becomes

$$q_{\mathrm{FM}\sigma} = \frac{1}{\pi\rho_0}\mathrm{Re}\{\tilde{G}_\sigma(\omega,R)\}. \tag{B5}$$

We can calculate this parameter rewriting the previous equation as

$$q_{\mathrm{FM}\sigma} = \frac{1}{\pi\rho_0}\tilde{G}_\sigma(\omega,R) - iA_\sigma(R), \tag{B6}$$

noting that the amplitude $A_\sigma(R)$ is already known from Eq. (32).

Thus, the quantity $\frac{1}{\pi\rho_0}\tilde{G}_\sigma(\omega,R)$ must be found to provide the relationship for the Fano parameter, which can be done using the decomposition

$$\frac{1}{\pi\rho_0}\tilde{G}_\sigma(\omega,R) = \frac{1}{2}\frac{\rho_{\mathrm{FM}\sigma}}{\rho_0}\sum_{l=1}^{2}\tilde{G}_l(\omega,R) \tag{B7}$$

written in terms of the integral

$$\tilde{G}_l(\omega,R) = \tfrac{1}{\pi}\int d\varepsilon_{k\sigma}\,H_0^{(l)}\left[k_{F\sigma}\left(1+\frac{\varepsilon_{k\sigma}}{D_\sigma}\right)R\right]\frac{\Gamma^2}{\Gamma^2+\varepsilon_{k\sigma}^2} \times \frac{1}{\omega-\varepsilon_{k\sigma}-i\eta}, \tag{B8}$$

which depends on the Hankel functions $H_0^{(1)}(z) = J_0(z) + iY_0(z)$ and $H_0^{(2)}(z) = J_0(z) - iY_0(z)$. We conclude that the task here reduces to evaluate the integrals $\tilde{G}_1(\omega,R)$ and $\tilde{G}_2(\omega,R)$.

The first integral is calculated by choosing a counterclockwise contour over a semicircle in the upper half of the complex plane that considers the simple pole $\varepsilon_{k\sigma} = +i\Gamma$. Following the residue theorem, we have

$$\tilde{G}_1(\omega,R) = H_0^{(1)}\left[k_{F\sigma}\left(1+i\frac{\Gamma}{D_\sigma}\right)R\right]\frac{\Gamma}{\omega-i\Gamma}. \tag{B9}$$

For the evaluation of the second integral, we used a clockwise contour over a semicircle in the lower half plane with poles placed at $\varepsilon_{k\sigma} = \omega - i\eta$ and $\varepsilon_{k\sigma} = -i\Gamma$, which leads to

$$\tilde{G}_2(\omega,R) = 2iH_0^{(2)}\left[k_{F\sigma}\left(1+\frac{\omega}{D_\sigma}\right)R\right]\frac{\Gamma^2}{\Gamma^2+\omega^2} + \frac{\Gamma}{\omega+i\Gamma} \times H_0^{(2)}\left[k_{F\sigma}\left(1-i\frac{\Gamma}{D_\sigma}\right)R\right]. \tag{B10}$$

As the complex-conjugate property $H_0^{(1)}(z^*) = [H_0^{(2)}(z)]^*$ is valid we are able to derive Eq. (30) from Eq. (B6) considering Eqs. (B7), (B9), and (B10) in the wide-band limit characterized by the conditions $\omega \ll D_\sigma$ and $\Gamma \ll D_\sigma$.

[1] A. C. Hewson, *The Kondo Problem to Heavy Fermions* (Cambridge University Press, Cambridge, 1993).
[2] D. Goldhaber-Gordon, H. Shtrikman, D. Mahalu, D. Abusch-Magder, U. Meirav, and M. A. Kastner, Nature (London) **391**, 156 (1998).
[3] S. M. Cronenwett, T. H. Oosterkamp, and L. P. Kouwenhoven, Science **281**, 540 (1998).
[4] K. Kang, S. Y. Cho, J. J. Kim, and S. C. Shin, Phys. Rev. B **63**, 113304 (2001).
[5] C. A. Busser, A. Moreo, and E. Dagotto, Phys. Rev. B **70**, 035402 (2004).
[6] A. Kogan, S. Amasha, D. Goldhaber-Gordon, G. Granger, M. A. Kastner, and Hadas Shtrikman, Phys. Rev. Lett. **93**, 166602 (2004).
[7] M. Sato, H. Aikawa, K. Kobayashi, S. Katsumoto, and Y. Iye, Phys. Rev. Lett. **95**, 066801 (2005).
[8] A. M. Lobos and A. A. Aligia, Phys. Rev. B **74**, 165417 (2006).
[9] A. C. Seridonio, M. Yoshida, and L. N. Oliveira, Europhys. Lett. **86**, 67006 (2009).
[10] A. C. Seridonio, M. Yoshida, and L. N. Oliveira, Phys. Rev. B **80**, 235318 (2009).
[11] M. Yoshida, A. C. Seridonio, and L. N. Oliveira, Phys. Rev. B **80**, 235317 (2009).
[12] V. Madhavan, W. Chen, T. Jamneala, M. F. Crommie, and N. S. Wingreen, Science **280**, 567 (1998).
[13] A. Schiller and S. Hershfield, Phys. Rev. B **61**, 9036 (2000).
[14] M. Plihal and J. W. Gadzuk, Phys. Rev. B **63**, 085404 (2001).
[15] H. C. Manoharan, C. P. Lutz, and D. M. Eigler, Nature (London) **403**, 512 (2000).
[16] V. Madhavan, W. Chen, T. Jamneala, M. F. Crommie, and N. S. Wingreen, Phys. Rev. B **64**, 165412 (2001).
[17] N. Knorr, M. A. Schneider, L. Diekhöner, P. Wahl, and K. Kern, Phys. Rev. Lett. **88**, 096804 (2002).
[18] P. Wahl, L. Diekhöner, G. Wittich, L. Vitali, M. A. Schneider, and K. Kern, Phys. Rev. Lett. **95**, 166601 (2005).
[19] Y. S. Fu, S. H. Ji, X. Chen, X. C. Ma, R. Wu, C. C. Wang, W. H. Duan, X. H. Qiu, B. Sun, P. Zhang, J. F. Jia, and Q. K. Xue, Phys. Rev. Lett. **99**, 256601 (2007).
[20] J. M. Aguiar-Hualde, G. Chiappe, E. Louis, and E. V. Anda, Phys. Rev. B **76**, 155427 (2007).
[21] G. Chiappe and E. Louis, Phys. Rev. Lett. **97**, 076806 (2006).
[22] O. Újsághy, J. Kroha, L. Szunyogh, and A. Zawadowski, Phys. Rev. Lett. **85**, 2557 (2000).
[23] A. F. Otte, M. Ternes, K. V. Bergmann, S. Loth, H. Brune, C. P. Lutz, C. F. Hirjibehedin, and A. J. Heinrich, Nat. Phys. **4**, 847 (2008).
[24] M. Ternes, A. J. Heinrich, and W. D. Schneider, J. Phys.: Condens. Matter **21**, 053001 (2009).
[25] J. Figgins and D. K. Morr, Phys. Rev. Lett. **104**, 187202 (2010).
[26] P. Wölfe, Y. Dubi, and A. V. Balatsky, Phys. Rev. Lett. **105**, 246401 (2010).
[27] H. Prüser, M. Wenderoth, P. E. Dargel, A. Weismann, R. Peters, T. Pruschke, and R. G. Ulbrich, Nat. Phys. **7**, 203 (2011).
[28] U. Fano, Phys. Rev. **124**, 1866 (1961).
[29] A. E. Miroshnichenko, S. F. Kivshar, and Y. S. Kivshar, Rev. Mod. Phys. **82**, 2257 (2010).
[30] K. R. Patton, S. Kettemann, A. Zhuravlev, and A. Lichtenstein, Phys. Rev. B **76**, 100408(R) (2007).
[31] A. C. Seridonio, F. M. Souza, and I. A. Shelykh, J. Phys.: Condens. Matter **21**, 095003 (2009).

[32] A. C. Seridonio, F. M. Souza, J. Del Nero, and I. A. Shelykh, Phys. E (Amsterdam) **41**, 1611 (2009).
[33] K. R. Patton, H. Hafermann, S. Brener, A. I. Lichtenstein, and M. I. Katsnelson, Phys. Rev. B **80**, 212403 (2009).
[34] N. Néel, J. Kröger, and R. Berndt, Phys. Rev. B **82**, 233401 (2010).
[35] P. Zhang, Q. K. Xue, Y. P. Wang, and X. C. Xie, Phys. Rev. Lett. **89**, 286803 (2002).
[36] Y. Qi, J. X. Zhu, S. Zhang, and C. S. Ting, Phys. Rev. B **78**, 045305 (2008).
[37] J. Martinek, M. Sindel, L. Borda, J. Barnaś, J. König, G. Schön, and J. von Delft, Phys. Rev. Lett. **91**, 247202 (2003).
[38] J. Martinek, Y. Utsumi, H. Imamura, J. Barnaś, S. Maekawa, J. König, and G. Schön, Phys. Rev. Lett. **91**, 127203 (2003).
[39] M. S. Choi, D. Sánchez, and R. López, Phys. Rev. Lett. **92**, 056601 (2004).
[40] J. Martinek, M. Sindel, L. Borda, J. Barnaś, R. Bulla, J. König, G. Schön, S. Maekawa, and J. von Delft, Phys. Rev. B **72**, 121302(R) (2005).
[41] Y. Utsumi, J. Martinek, G. Schön, H. Imamura, and S. Maekawa, Phys. Rev. B **71**, 245116 (2005).
[42] R. Świrkowicz, M. Wilczyński, M. Wawrzyniak, and J. Barnaś, Phys. Rev. B **73**, 193312 (2006).
[43] A. N. Pasupathy, R. C. Bialczak, J. Martinek, J. E. Grose, L. A. K. Donev, P. L. McEuen, and D. C. Ralph, Science **306**, 86 (2004).
[44] M. Sindel, L. Borda, J. Martinek, R. Bulla, J. König, G. Schön, S. Maekawa, and J. von Delft, Phys. Rev. B **76**, 045321 (2007).
[45] K. Hamaya, M. Kitabatake, K. Shibata, M. Jung, M. Kawamura, K. Hirakawa, T. Machida, and T. Taniyama, Appl. Phys. Lett. **91**, 232105 (2007).
[46] K. Hamaya, M. Kitabatake, K. Shibata, M. Jung, M. Kawamura, S. Ishida, T. Taniyama, K. Hirakawa, Y. Arakawa, and T. Machida, Phys. Rev. B **77**, 081302(R) (2008).
[47] M. R. Calvo, J. Fernádez-Rossier, J. J. Palacios, D. Jacob, D. Natelson, and C. Untiedt, Nature (London) **458**, 1150 (2009).
[48] J. Hauptmann, J. Paaske, and P. Lindelof, Nat. Phys. **4**, 373 (2008).
[49] S.L. Kawahara, J. Lagoute, V. Repain, C. Chacon, Y. Girard, J. Klein, and S. Rousset, Phys. Rev. B **82**, 020406(R) (2010).
[50] J. Nygard, W. F. Koehl, N. Mason, L. DiCarlo, and C. M. Marcus, e-print arXiv:cond-mat/0410467.
[51] I. Weymann and L. Borda, Phys. Rev. B **81**, 115445 (2010).
[52] I. Weymann, Phys. Rev. B **83**, 113306 (2011).
[53] M. Misiorny, I. Weymann, and J. Barnaś, Phys. Rev. Lett. **106**, 126602 (2011).
[54] M. Gaass, A. K. Hütel, K. Kang, I. Weymann, J. von Delft, and Ch. Strunk, Phys. Rev. Lett. **107**, 176808 (2011).
[55] M. Misiorny, I. Weymann, and J. Barnaś, Phys. Rev. B **84**, 035445 (2011).
[56] P. W. Anderson, Phys. Rev. **124**, 41 (1961).
[57] T. Lobo, M. S. Figueira, and M. E. Foglio, Nanotechnology **17**, 6016 (2006).
[58] M. E. Foglio, T. Lobo, and M. S. Figueira, e-print arXiv:0903.0139.
[59] T. Lobo, M. S. Figueira, and M. E. Foglio, Nanotechnology **21**, 274007 (2010).
[60] Recently, though, it was found low Kondo temperatures (2.6 K) in a STM metallic system, comparable to typical T_K in QDs (see Ref. 23).
[61] J. Friedel, Adv. Phys. **3**, 446 (1954).
[62] F. Mezei and A. Zawadowski, Phys. Rev. B **3**, 167 (1971).
[63] J. Friedel, Nuovo Cimento Suppl. **7**, 287 (1958).
[64] J. Hubbard, Proc. R. Soc. A **77**, 237 (1964).
[65] M. S. Figueira, M. E. Foglio, and G. G. Martinez, Phys. Rev. B **50**, 17933 (1994).
[66] B. R. Alascio, R. Allub, and A. Aligia, J. Phys. C: Solid State Phys. **13**, 2869 (1980).
[67] D. D. Langreth, Phys. Rev. **150**, 516 (1966).
[68] R. Bulla, T. A. Costi, and T. Pruschke, Rev. Mod. Phys. **80**, 395 (2008).
[69] D. N. Zubarev, Sov. Phys.–Uspekhi **3**, 320 (1960).